IEEE Access
Multidisciplinary | Rapid Review | Open Access Journal

Received 30 November 2023, accepted 1 January 2024, date of publication 5 January 2024,
date of current version 12 January 2024.

Digital Object Identifier 10.1109/ACCESS.2024.3350191

RESEARCH ARTICLE

Model Predictive Based Direct Power Control Method Using Switching State Preference for Independent Phase Loss Decrease of Three-Phase Pulsewidth Modulation (PWM) Rectifiers

MINH HOANG NGUYEN[1], SANGSHIN KWAK[1], (Member, IEEE), AND SEUNGDEOG CHOI[2], (Senior Member, IEEE)

[1]School of Electrical and Electronics Engineering, Chung-Ang University, Seoul 06974, South Korea
[2]Department of Electrical and Computer Engineering, Mississippi State University, Starkville, MS 39762, USA

Corresponding author: Sangshin Kwak (sskwak@cau.ac.kr)

This work was supported in part by the National Research Foundation of Korea (NRF) Grant funded by the Korea Government, Ministry of Science and ICT (MSIT), under Grant 2020R1A2C1013413; and in part by Korea Electric Power Corporation under Grant R21XO01-3.

ABSTRACT Nowadays, active rectifiers are increasingly used, particularly in grid-connected applications. The high efficiency and reliability of active rectifiers become crucial for increasing the system performance. Due to the lack of model predictive control methods considering the different aging levels among phase legs of rectifiers, this paper thus introduces a direct power control-based model predictive control for independent loss reduction in each phase of the active rectifier. Different from conventional techniques, the target of proposed model predictive direct power control scheme is lowering switching loss in the leg having highest aging level of active rectifier, resulting in increasing its corresponding lifetime and lifetime of entire rectifier. As opposed to the model predictive control method based on incorporating additional terms regarding switching loss in the cost function, a switching state preselection strategy is proposed in this study to determine clamping region and corresponding preselected switching state for the leg having highest aging level of active rectifier. The use of the proposed method lowers thermal stress in the leg having highest aging level and increases lifetime of active rectifier. Simulation and experimental results for the proposed technique are presented and compared with conventional model predictive direct power control method to validate the accuracy and feasibility of the proposed method.

INDEX TERMS Active rectifier, predictive control, direct power control, per-phase, lifetime.

I. INTRODUCTION

In the scope of power electronics, three-phase active rectifiers find extensive application in the conversion of ac power into dc power for a variety of uses, such as driving motors, powering renewable energy systems, and propelling electric vehicles. Employing a pulse-width modulation (PWM) strategy, a three-phase active rectifier offers a solution that overcomes the limitations of phase-control methods and passive diode rectifiers [1]. However, this topology faces significant challenges, including high switching losses and the need for large passive components such as inductors and capacitors. Accordingly, traditional rectifier systems suffer from disadvantages such as reduced efficiency, lower power density, and increased electromagnetic interference levels [2]. Switching losses are the energy losses experienced by power devices as they change their corresponding state. These losses not only compromise system efficiency and reliability but can also subject the power devices to thermal stress, potentially leading to premature failure [3], [4]. Additionally, suffering high thermal stress will significantly lower the lifetime of power semiconductors and entire active rectifier. Thus,

The associate editor coordinating the review of this manuscript and approving it for publication was Inam Nutkani.

effectively managing switching losses in active rectifiers represents a vital aspect of design and control in power systems.

To improve the rectifier efficiency, it is essential to decrease the power loss generated by power switches, where switching loss accounts for the majority. One technique for mitigating these losses is the application of soft-switching methods. In [5] and [6], the authors propose a method that utilizes increased current ripple to discharge the voltage across the switches before activating them. Unfortunately, this approach requires additional passive components in the resonant circuit, which negatively impacts system reliability and increases costs. In [7], the authors propose a diode rectifier system, including an instantaneous reactive power compensator (IRPC) and a buck converter without using any dc energy storage components. The IRPC serves to lower harmonic currents by supplying only the ac components of reactive power. This results in a compensatory current that is typically reduced to 32% of the grid current, thereby reducing power losses in the power switches. Nevertheless, these methods are intricate and challenging to apply in real-world systems. Making adjustment to the modulation algorithm, without requiring extra hardware, offers a straightforward way to implement improvements in practical systems. In [8] and [9], the authors introduce control schemes that adjust modulation voltages by adding proper offset voltages, resulting in discontinuous PWMs (DPWMs). These DPWM methods can decrease the switching frequency by clamping one converter phase to either the upper or lower dc-link. However, it is important to note that this may potentially lead to a degradation in the performance of the active rectifiers.

Recently, model predictive control (MPC) has been applied extensively as a control strategy to numerous electronic devices, converters, and drives due to several desirable characteristics, including fast dynamic response, lack of modulator, easy inclusion of nonlinearities, and constraints of the system, ability to incorporate nested control loops into a single loop, and flexibility to include other system requirements in the controller. The finite control-set MPC algorithms can be classified into four main kinds: model predictive current control (MPCC), model predictive virtual flux control (MPVFC), model predictive direct power control (MPDPC), and model predictive virtual flux direct power control (MPVFDPC). The difference between these control schemes is the variables. The MPCC scheme [10] directly regulates the input currents of active rectifier by employing the input currents as a control variable. In contrast, the MPVFC method [11], [12] uses the virtual flux of the input voltages. Meanwhile, the MPDPC [13], [14] and MPVFDPC techniques [15], [16] regulate the input powers. By using MPC, the author in [17] proposes a cascaded dual-MPC algorithm that reduces the switching losses of active rectifier. This technique only uses predictive switching states that allow two or fewer switches to commutate at each sampling instant, whereas eliminated predictive switching states have either four or six switches commutating at the same time. However, there is no information on switching loss reduction performance in this study. Another method detailed in [18], named predictive hybrid PWM, dynamically chooses the suitable PWM sequence by employing a predictive algorithm. As reported in this study, the predictive hybrid PWM method can reduce switching losses by up to 23% compared to conventional space vector PWM, though there is no comparison to the conventional MPC technique. Additionally, an MPDPC with voltage vectors preselection technique in [19] decreases the switching loss of the active rectifier by using preselected rectifier voltage vectors instead of all possible ones. However, the reduction of switching losses is only around 10% and decreases when the sampling period increases.

Although several techniques were developed to increase the efficiency and reliability of active rectifier, the thermal control methods mentioned earlier fail to consider that the phase legs of the active rectifier can have different aging levels. Within three-phase active rectifiers, it is possible for each individual phase leg to experience varying aging levels or have distinct expected lifetimes. These discrepancies can arise from unequal thermal stress or from the prior replacement of a failed switch. Furthermore, the manufacturing process is also recognized as a cause of power device failures. The active rectifier will stop working when a single power switch is broken. Hence, the corresponding lifetime of entire active rectifier is decided by the durability of the leg having highest aging level. The author in [20] proposes a modified carrier-based PWM for individual phase loss reduction, which can decrease by about 46.5% switching loss for a specific leg in comparison to the conventional PWM method. In [21] and [22], the author proposed per-phase MPC techniques with offset voltage injection and selected switching states strategies, respectively, to prolong the lifetime of the most aged leg in a two-level voltage source inverter. However, to the author's knowledge, there is no study of the MPC technique to reduce switching loss in an individual phase for active rectifier. Although the switching frequency or even power loss can be added to the cost function as an extra term in MPC to reduce loss, it is not ease to strike a balance with the primary control focused on improving efficiency through the design of optimal weighting factors [23].

In this study, an MPC technique based-direct power control combined with a switching state preselection strategy for independent loss reduction in each phase of active rectifier is proposed. The proposed technique uses instantaneous real and reactive powers to evaluate the optimal switching states. Thus, the virtual filter in [24] might be investigated to include in the power control part of MPDPC method to filter the calculated power to achieve more accurate control. Different from the conventional MPDPC method and previous reducing switching loss MPC strategies, the target of proposed MPDPC is reducing the switching loss in the leg having highest aging level of active rectifier, resulting in increasing its corresponding lifetime and lifetime of entire rectifier. The proposed per-phase MPDPC method does not need additional terms corresponding to switching loss in

the cost function and does not require additional hardware but uses a switching state preselection strategy instead. This switching state preselection strategy identifies the clamping regions of the leg having highest aging level and the associated switching states among available voltage vectors of active rectifier. Different from the modified carrier-based PWM (CBPWM) method in [20], the total clamping region in the leg having highest aging level leg could be up to two-thirds fundamental period, which allows achieving minimum switching loss when employing the proposed technique. Thus, the switching loss in the leg having highest aging level can be reduced by only considering preselected switching states that avoid changing the current switching state. This leads to the decrease of thermal stress in the leg having highest aging level, resulting in an increased lifetime of the corresponding leg and entire active rectifier. Additionally, the proposed per-phase MPDPC technique does not degrade the output performance of active rectifier and can be readily employed in practical systems without diminishing its effectiveness. However, the trade-off between reducing power loss in only one phase leg and maintaining the output current total harmonic distortion (THD) performance is the increased power loss in the remaining phase legs. Hence, the total loss in comparison between the proposed method and the conventional MPDPC method is similar. As indicated in previous studies [25], [26], the operation of the converter connecting to a weak grid might be affected by the phase-locked loop (PLL) system, which may not estimate the correct phase angle of the grid voltage during the transient or even destabilizes the system. However, the proposed per-phase MPDPC method is based on direct power control, which removes the need for the PLL system but uses instantaneous real and reactive powers. Hence, the converter connecting to a weak grid using the proposed method can be correctly operated. Additionally, in terms of the dc output current, due to the clamping regions generated by proposed method to reduce switching loss in the specific phase leg, the dc output current ripple might increase compared to the conventional MPDPC method. However, the use of a large capacitor at dc output side can mitigate these ripples of dc output current but increase the cost of the entire system. When using the dc output current as the control objective in the PI controller, the high current ripple might exert a negative impact on the controller. Thus, the use of current reconstruction considering current ripple [27] should be considered to ensure the proper operation of the current controller.

As for the proposed per-phase MPDPC method, it requires determining the most aged phase leg. The diagnosis methods require the aging indicator to identify the current aging status of the power semiconductor devices. Aging indicator identification on power semiconductor devices has been carried out by performing accelerated aging experiments with monitoring of selected parameters. Accelerated aging tests allow the effects of failure mechanisms to be analyzed and aging indicators to be identified. Various electrical aging indicators for IGBT have been investigated and proposed in the literature, such as changes in collector-emitter on-state voltage $V_{ce,on}$ [28], [29], and threshold voltage V_{th} [30], [31], and temperature [32], [33], [34]. However, the diagnosis method is out of the scope of this study, a detailed description is not included.

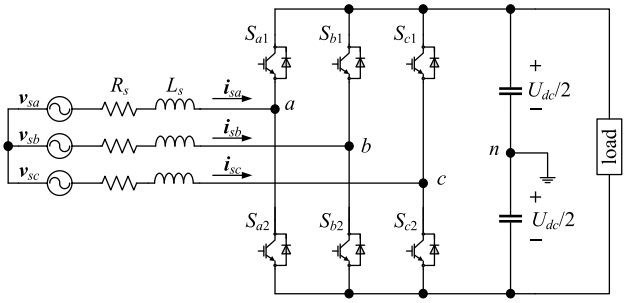

FIGURE 1. Three-phase active rectifier.

The proposed technique is demonstrated by the simulation and experimental findings in comparison to the conventional MPDPC method in a three-phase active rectifier system.

II. CONVENTIONAL MPDPC FOR ACTIVE RECTIFIER

The active rectifier can be represented by the model depicted in Fig. 1. The active rectifier comprises six power switches connected to the three-phase supply voltage $v_{sx}(x = a, b, c)$ using the line inductances L_s and resistances R_s.

The dynamic description of input current can be expressed as follows:

$$L_s \frac{di_{sx}}{dt} = v_{sx} - v_{\mathrm{AR}} - R_s i_{sx} \ (x = a, b, c) \tag{1}$$

where i_{sx} is the input current, v_{sx} is the input voltage, and $v_{\mathrm{A.R.}}$ is the voltage generated by the rectifier. The input current dynamics in (1) can be expressed in vector form in $\alpha\beta$ frame by transforming the input voltages and currents as follows:

$$\boldsymbol{v}_s = \frac{2}{3}(v_{sa} + v_{sb}e^{j\left(\frac{2\pi}{3}\right)} + v_{sc}e^{j\left(\frac{4\pi}{3}\right)} \tag{2}$$

$$\boldsymbol{i}_s = \frac{2}{3}(i_{sa} + i_{sb}e^{j\left(\frac{2\pi}{3}\right)} + i_{sc}e^{j\left(\frac{4\pi}{3}\right)} \tag{3}$$

Hence, (1) becomes.

$$L_s \frac{d\boldsymbol{i}_s}{dt} = \boldsymbol{v}_s - v_{\mathrm{AR}} - R_s \boldsymbol{i}_s \tag{4}$$

The voltage $v_{\mathrm{A.R.}}$ is determined by the switching state and the dc output voltage, which is described as follows:

$$\boldsymbol{v}_{\mathrm{AR}} = \left(\frac{2}{3}(S_a + S_b e^{j\left(\frac{2\pi}{3}\right)} + S_c e^{j\left(\frac{4\pi}{3}\right)}\right) U_{dc} \tag{5}$$

where S_a, S_b, and S_c are the switching states of upper switches in corresponding legs, as depicted in Fig. 1. When $S_x = 0$, the upper switch is OFF, whereas $S_x = 1$ means the upper switch is ON $(x = a, b, c)$.

By applying forward Euler approximation with a sampling period T_{sp}, (4) can be expressed in discrete-time form as

$$\boldsymbol{i}_s(k+1) = \left(1 - \frac{R_s T_{sp}}{L_s}\right)\boldsymbol{i}_s(k) + \frac{T_{sp}}{L_s}\left[\boldsymbol{v}_s(k) - \boldsymbol{v}_{\mathrm{AR}}(k)\right] \tag{6}$$

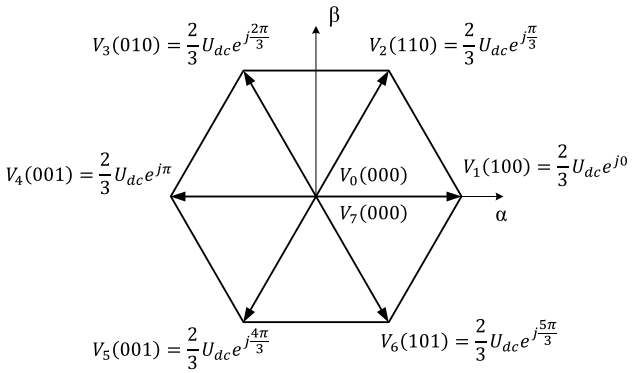

FIGURE 2. Active rectifier's voltage vectors.

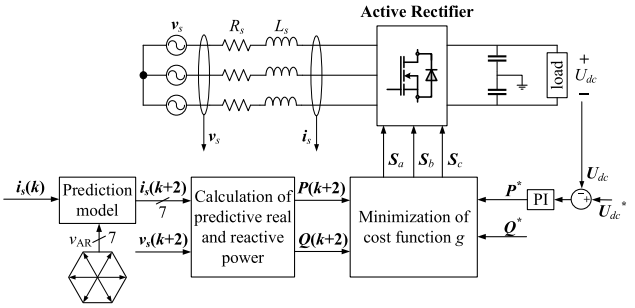

FIGURE 3. Conventional MPDPC.

To avoid control delay of the implementation of MPC in practical applications, delay compensation should be applied. The predictive input current at $(k+2)^{\text{th}}$ instant is generated by shifting $\boldsymbol{i}_s\,(k+1)$ one step forward as follows:

$$\boldsymbol{i}_s\,(k+2) = \left(1 - \frac{R_s T_{sp}}{L_s}\right)\boldsymbol{i}_s\,(k+1) + \frac{T_{sp}}{L_s}\left[\boldsymbol{v}_s\,(k+1) - \boldsymbol{v}_{\text{AR}}(k+1)\right] \tag{7}$$

The predictive instantaneous input real and reactive power are calculated as

$$P\,(k+2) = v_{s\alpha}\,(k+2)\,i_{s\alpha}\,(k+2) + v_{s\beta}\,(k+2)\,i_{s\beta}\,(k+2) \tag{8}$$

$$Q\,(k+2) = v_{s\beta}\,(k+2)\,i_{s\alpha}\,(k+2) - v_{s\alpha}\,(k+2)\,i_{s\beta}\,(k+2) \tag{9}$$

where $v_{sx}\,(k+2)\,(x = \alpha, \beta)$ and $i_{sx}\,(k+2)\,(x = \alpha, \beta)$ are the predictive input voltages and currents at $(k+2)^{\text{th}}$ sampling instant in the $\alpha\beta$ frame. In conventional MPDPC, out of the eight possibilities of predictive input real power and reactive power acquired by the eight vectors $\boldsymbol{v}_{\text{AR}}$, as shown in Fig. 2, one voltage vector, which corresponds to the smallest value of cost function, is chosen. The cost function of power control is specified as follows:

$$g = \left|P^*\,(k+2) - P(k+2)\right| + \left|Q^*\,(k+2) - Q(k+2)\right| \tag{10}$$

In the MPDPC, the output dc voltage U_{dc} is controlled by employing a PI controller. The output of the PI controller is the reference real power P^*. Meanwhile, the reference reactive power Q^* is usually set to zero or desired values based on specific applications. Fig. 3 depicts the diagram of conventional MPDPC technique.

III. PROPOSED PER-PHASE MPDPC METHOD WITH SWITCHING STATE PRESELECTION STRATEGY

Based on the previously discussed analysis, the individual legs of active rectifier may experience different aging levels caused by the manufacturing process, uneven distribution of thermal stress, and prior replacement during maintenance. Consequently, there can be disparities in the lifetime between legs. Given that the active rectifier will stop functioning if any of the phase legs fails, it becomes essential to extend the lifetime of the leg having the highest aging level.

The target of proposed per-phase MPDPC with switching state preselection strategy is lowering the switching loss in the leg having highest aging level of active rectifier, resulting in increasing its corresponding lifetime and lifetime of entire rectifier. Different from the conventional MPDPC method where all eight vectors $\boldsymbol{v}_{\text{AR}}(k+1)$ are used to predict the predictive input powers, the proposed per-phase MPDPC technique will use two different rectifier voltage vector sets. In the first rectifier voltage vector set, all rectifier voltage vectors will be used as in conventional MPDPC method. Meanwhile, in the second rectifier voltage vector set, the proposed per-phase MPDPC method eliminates four vectors that would result in significant switching loss in the next sampling instant. The remaining four voltage vectors involve clamping the leg having highest aging level of active rectifier to either the positive or negative dc-link to keep this leg from changing its switching state. This leads to a decrease in the switching loss of the leg having highest aging level.

The rectifier voltage vectors in the second set used for predicting the predictive input real and reactive power are preselected based on the reference rectifier voltage. The predictive reference rectifier voltage $\boldsymbol{v}^*_{\text{AR}}\,(k+1)$ in $\alpha\beta$ frame is calculated by inversing the current dynamic in (7) as follows:

$$v^*_{\text{AR}\alpha}\,(k+1) = v_{s\alpha}\,(k+1) + \frac{L_s}{T_{sp}}\left\{\left(1 - \frac{R_s T_{sp}}{L_s}\right) i^*_{s\alpha}\,(k+1) - i^*_{s\alpha}\,(k+2)\right\} \tag{11}$$

$$v^*_{\text{AR}\beta}\,(k+1) = v_{s\beta}\,(k+1) + \frac{L_s}{T_{sp}}\left\{\left(1 - \frac{R_s T_{sp}}{L_s}\right) i^*_{s\beta}\,(k+1) - i^*_{s\beta}\,(k+2)\right\} \tag{12}$$

Although the predictive reference rectifier voltage in (11) and (12) can be calculated using actual input currents, this might introduce a delay in sampling instant. Hence, the predictive reference input current is used to calculate the predictive reference rectifier voltage. The predictive reference

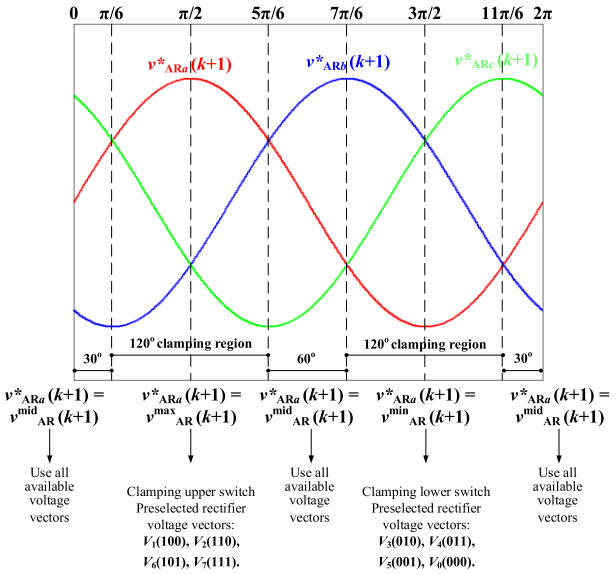

FIGURE 4. Clamping regions and preselected rectifier voltage vectors, when considering phase-a is the leg having highest aging level.

input current is calculated by using reference real and reactive power, as follows:

$$i^*_{s\alpha}(k+2) = \left(\frac{v_{s\alpha}(k+2)}{V^2_{peak}}\right) \times \left(P^*(k+2) + Q^*(k+2)\frac{v_{s\beta}(k+2)}{v_{s\alpha}(k+2)}\right) \quad (13)$$

$$i^*_{s\beta}(k+2) = \left(\frac{v_{s\beta}(k+2)}{V^2_{peak}}\right) \times \left(P^*(k+2) + Q^*(k+2)\frac{v_{s\alpha}(k+2)}{v_{s\beta}(k+2)}\right) \quad (14)$$

where V_{peak} is the peak value of the input phase voltage. Once the predictive rectifier voltage vector is generated by using (11). After generating the predictive reference rectifier voltage by substituting reference input currents in (13) and (14) to (11) and (12), the predictive reference rectifier voltage in $\alpha\beta$ frame will be transformed to $v^*_{\mathrm{AR}a}(k+1)$, $v^*_{\mathrm{AR}b}(k+1)$, and $v^*_{\mathrm{AR}c}(k+1)$ in abc frame. The three-phase predictive reference rectifier voltages are sorted depending on their instantaneous magnitude as follows:

$$v^{\max}_{\mathrm{AR}}(k+1) = \max\left[v^*_{\mathrm{AR}a}(k+1), v^*_{\mathrm{AR}b}(k+1), v^*_{\mathrm{AR}c}(k+1)\right] \quad (15)$$

$$v^{\mathrm{mid}}_{\mathrm{AR}}(k+1) = mid\left[v^*_{\mathrm{AR}a}(k+1), v^*_{\mathrm{AR}b}(k+1), v^*_{\mathrm{AR}c}(k+1)\right] \quad (16)$$

$$v^{\min}_{\mathrm{AR}}(k+1) = \min\left[v^*_{\mathrm{AR}a}(k+1), v^*_{\mathrm{AR}b}(k+1), v^*_{\mathrm{AR}c}(k+1)\right] \quad (17)$$

TABLE 1. The second rectifier voltage vector set for aged leg.

Aged leg	Condition	Clamping switch	Preselected rectifier voltage vector set
Phase-*a*	$v_{\mathrm{AR}a}(k+1) = v^{\max}_{\mathrm{AR}}(k+1)$	Upper switch	Set 2a: $V_1(100)$,$V_2(110)$, $V_6(101)$, $V_7(111)$
	$v_{\mathrm{AR}a}(k+1) = v^{\min}_{\mathrm{AR}}(k+1)$	Lower switch	Set 2b: $V_0(000)$,$V_3(010)$, $V_4(011)$, $V_5(001)$
Phase-*b*	$v_{\mathrm{AR}b}(k+1) = v^{\max}_{\mathrm{AR}}(k+1)$	Upper switch	Set 2a: $V_2(110)$,$V_3(010)$, $V_4(011)$, $V_7(111)$
	$v_{\mathrm{AR}b}(k+1) = v^{\min}_{\mathrm{AR}}(k+1)$	Lower switch	Set 2b: $V_0(000)$, $V_1(100)$, $V_5(001)$, $V_6(101)$
Phase-*c*	$v_{\mathrm{AR}c}(k+1) = v^{\max}_{\mathrm{AR}}(k+1)$	Upper switch	Set 2a: $V_4(011)$, $V_5(001)$, $V_6(101)$, $V_7(111)$
	$v_{\mathrm{AR}c}(k+1) = v^{\min}_{\mathrm{AR}}(k+1)$	Lower switch	Set 2b: $V_0(000)$, $V_1(100)$, $V_2(110)$, $V_3(010)$

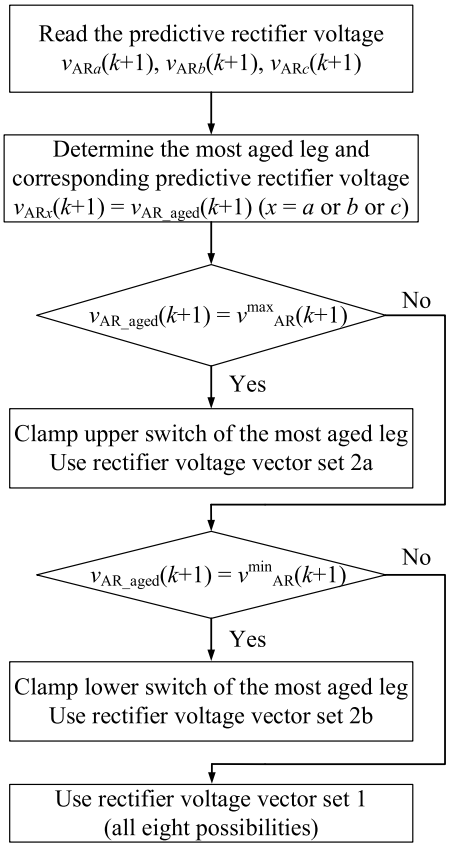

FIGURE 5. Block diagram of switching state preselection strategy.

When the magnitude of the predictive reference rectifier voltage has medium voltage $v^{\mathrm{mid}}_{\mathrm{AR}}(k+1)$, the clamping must be avoided in that prohibitive phase to ensure that the active rectifier is not operated in overmodulation region. On the other hand, if the predictive reference rectifier voltage of the leg having highest aging level is maximum voltage $v^{\max}_{\mathrm{AR}}(k+1)$ or minimum voltage $v^{\max}_{\mathrm{AR}}(k+1)$, the leg having

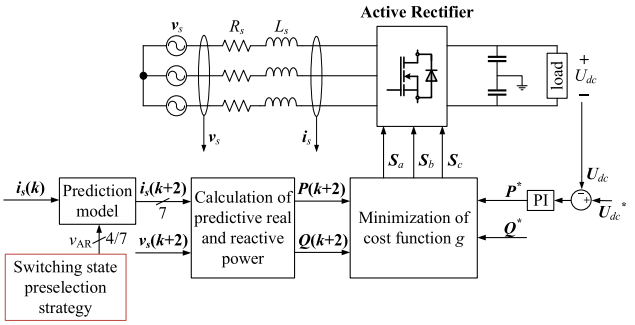

FIGURE 6. Proposed per-phase MPDPC technique with switching state preselection strategy block control.

TABLE 2. Active rectifier parameters.

Parameter	Value
Input phase voltage (V_{peak})	80
Line resistance (Ω)	0.1
Line inductance (mH)	15
dc-link capacitance (μF)	1100
Load resistance (Ω)	100
Sampling time (μs)	50
dc-link output voltage (V)	220
Input real power reference (W)	500

highest aging level will be clamped to positive or negative dc-link, respectively. Fig. 4 illustrates the case that phase-a is the leg having highest aging level. The clamping regions of phase-a correspond to two period that $v^*_{\mathrm{AR}a}(k+1) = v^{\max}_{\mathrm{AR}}(k+1)$ and $v^*_{\mathrm{AR}a}(k+1) = v^{\min}_{\mathrm{AR}}(k+1)$. It can be noticed that the clamping regions in positive and negative dc-link can achieve one third fundamental period. This leads to the total clamping region of the leg having highest aging level can achieve two thirds fundamental period, equals to 240° period of time. In these two clamping regions, the rectifier voltage vectors, which maintain the current switching state of phase-a will be preselected.

Table 1 lists these preselected rectifier voltage vectors in the second set. In the second rectifier voltage vector set, set 2a includes the rectifier voltage vectors that make the upper switch in the leg having highest aging level always ON. Alternatively, set 2b includes the rectifier voltage vectors that make the lower switch in the leg having highest aging level always ON. By employing these rectifier voltage vectors in the second set during clamping regions, the switches in the leg having highest aging level will be avoided from changing state, resulting in a reduction of switching losses.

Fig. 5 illustrates the diagram of switching state preselection strategy, and Fig. 6 depicts the whole block control of proposed per-phase MPDPC with switching state preselection strategy. As can be seen in Fig. 6, the difference between the proposed technique and the conventional MPDPC method is the switching state preselection strategy block.

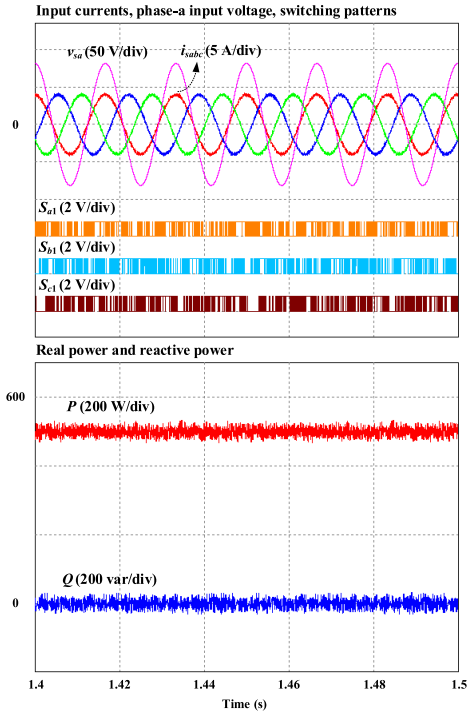

FIGURE 7. Simulation waveform under steady-state condition obtained by (a) the conventional MPDPC, (b) proposed per-phase MPDPC with switching state preselection strategy.

IV. DEMONSTRATION RESULTS

A. SIMULATION RESULTS

The proposed per-phase MPDPC with switching state preselection strategy is conducted in simulation environment

(a)

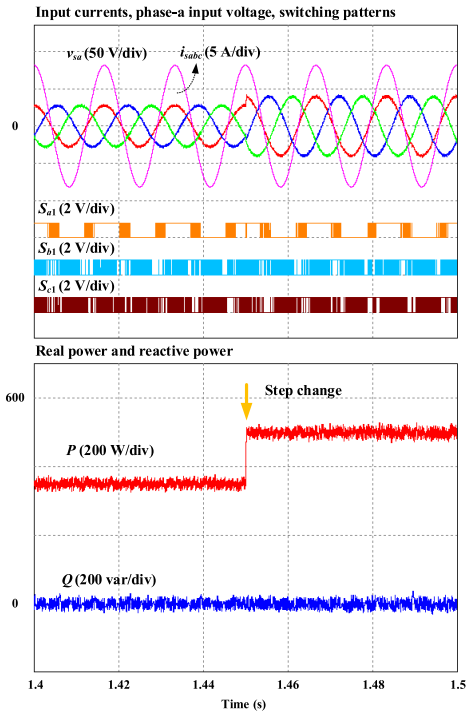

(b)

FIGURE 8. Simulation waveform under transient-state condition with increase of real power reference obtained by (a) the conventional MPDPC, (b) proposed per-phase MPDPC with switching state preselection strategy.

using the PSIM simulation program. The simulation result of the proposed technique is compared with the conventional MPDPC method to verify its performance. In the simulation, phase-a is considered as the leg to have the highest aging level. The parameters of the active rectifier system are listed in Table 2. The design considerations of the inductor and capacitor for the active rectifier are followed by the design guide for rectifier TIDM-1000 from Texas Instrument and available equipment in the laboratory [35]. The value of the inductor is determined by the following parameters, including the dc-link output voltage and input voltage, the switching frequency, and the current ripple needed. The value of input inductor is calculated as follows

$$L_s = \frac{U_{dc}/2}{4 \times f_{sw} \times \Delta i_{pp,max}} \tag{18}$$

where $\Delta i_{pp,max}$ is the maximum ripple of input current. Due to the active rectifier being operated under a low switching frequency, the large inductor value is selected in this study to achieve the desired current ripple.

Fig. 7 illustrates the simulation waveforms of the conventional MPDPC and proposed per-phase MPDPC with switching state preselection strategy, including phase-a input voltage, input currents, switching patterns, and actual real and reactive powers.

In Fig. 7(a) and (b), the input currents are sinusoidal. Unity power factor is achieved since the input current is in phase with the input voltage. In both Fig. 7(a) and (b), the actual real and reactive power correctly track their reference values at $P^* = 500$W and $Q^* = 0$var, respectively. Both conventional and proposed methods exhibit similar ripples in actual real and reactive power. As for switching patterns shown in Fig. 7(a), the switching pattern of phase-a contains clamping regions, where the switches in phase-a are prevented from changing the current state. These clamping regions have a value of one-third of the fundamental period, which leads to the total clamping region of phase-a is 240°. This allows the leg having the highest aging level to achieve the minimum switching loss, resulting in an increasing corresponding lifetime. These clamping regions are the difference between the proposed MPDPC method with switching state preselection strategy and the conventional method.

The dynamic performance of two control scheme is assessed in Fig. 8, where a step change in the reference real power P^* is made, shifting from 350W to 500W. As shown in Fig. 8, both two control schemes achieve similar power tracking capability. Additionally, the real and reactive powers show no coupling in two control schemes. In Fig. 8(b), the switching pattern of phase-a includes correct clamping regions of 120° even during the transient-state.

Fig. 9 displays the dynamic response when the reactive power reference Q^* is altered, transitioning from 0 var to 150var, while keeping the reference real power fixed at $P^* = 500$W. As shown in Fig. 9, both two control schemes achieve similar power tracking capability. The phase difference between input current and input voltage changes correctly following the rise of reactive power. The switching pattern of phase-a has correct clamping regions of 120° even during the transient-state. The simulation results verify that

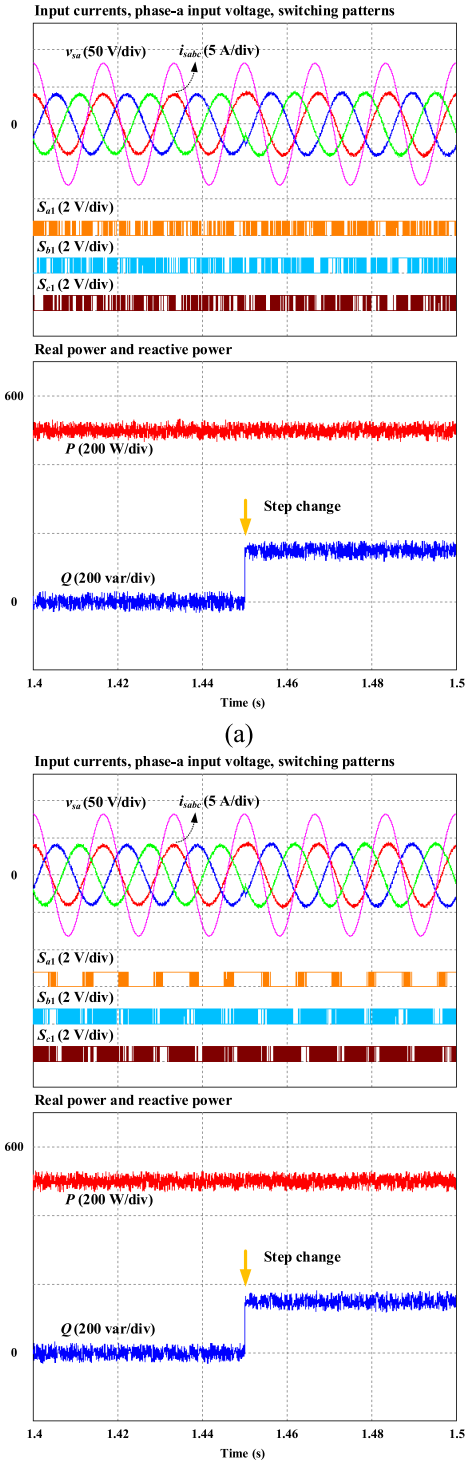

FIGURE 9. Simulation waveform under transient-state condition with increase of reactive power reference obtained by (a) the conventional MPDPC, (b) proposed per-phase MPDPC with switching state preselection strategy.

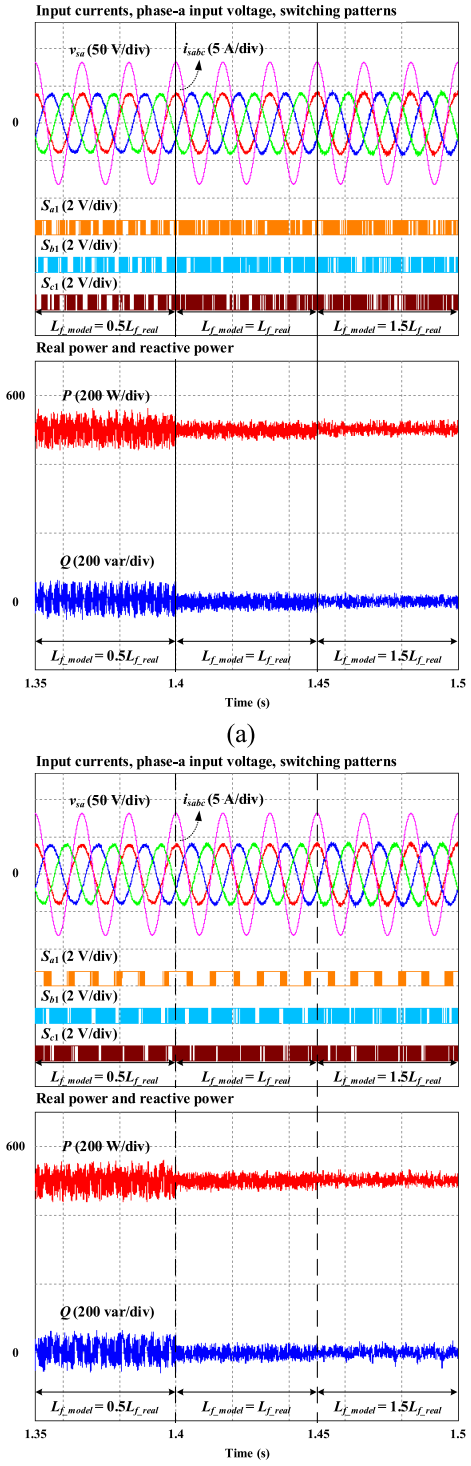

FIGURE 10. Simulation waveform under line inductance uncertainty obtained by (a) the conventional MPDPC, (b) proposed per-phase MPDPC with switching state preselection strategy.

the proposed per-phase MPDPC operates correctly in both steady-state and transient state.

Parameter uncertainty can degrade the control system performance and even affect system stability. In MPC technique, the prediction model critically relies on having accurate system parameters. Fig. 10 shows the behavior of active rectifier under line inductance uncertainty obtained by the conventional and proposed method.

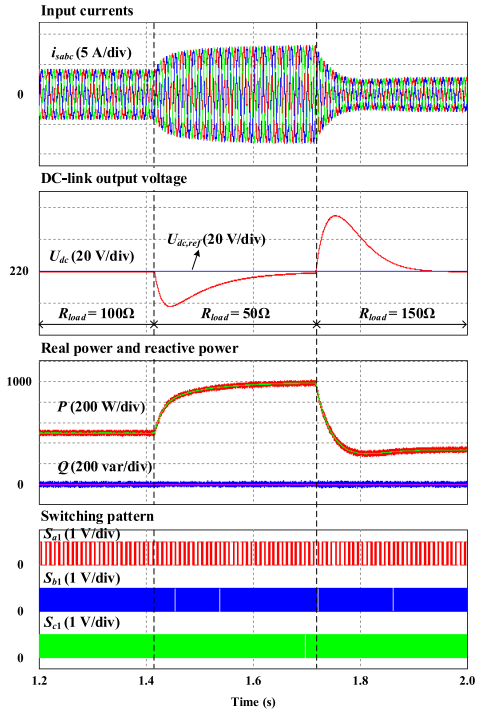

FIGURE 11. Simulation waveform under load variation obtained by proposed per-phase MPDPC with switching state preselection strategy.

In the first part of waveforms, the model line inductance is half of real line inductance ($L_{s,model} = 0.5L_{s,real}$); the middle shows the model line inductance is correct ($L_{s,model} = L_{s,real}$); and the last shows that the model line inductance is 1.5 times higher than the real one ($L_{s,model} = 1.5L_{s,real}$). In Fig. 10(a) and (b), both conventional and proposed methods properly control the input currents with accurate magnitude and phase. However, it can be noticed that in both conventional and proposed techniques, the ripple in real and reactive powers under $L_{s,model} = 0.5L_{s,real}$ condition is significantly higher than that of normal condition and $L_{s,model} = 1.5L_{s,real}$ condition.

Fig. 11 displays the simulation waveforms under load variation conditions obtained by the proposed per-phase MPDPC with switching state preselection strategy. As shown in Fig. 11, the dc-link output voltage correctly tracks the corresponding reference under the variation in magnitude of resistance load. The input currents and real power change properly according to the variation of resistance load. Meanwhile, the switching pattern of phase-a contains a correct clamping region of 120°. It validates that the proposed per-phase MPDPC with switching state preselection strategy operates correctly in spite of the change of output load.

B. EXPERIMENTAL RESULTS

To further confirm the precision of the proposed per-phase MPDPC with switching state preselection strategy, an experimental setup for an active rectifier prototype has been constructed, as depicted in Fig. 12. Bidirectional switches

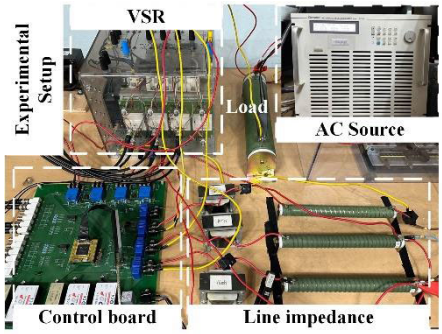

FIGURE 12. Experimental prototype of active rectifier.

using common IGBTs are employed. The conventional and proposed MPDPC schemes are employed by TI DSP TMS320F28335. The programmable source CHROMA 61702 is used as input supply ac voltage. The parameters and conditions align with those presented in the simulation section.

Fig. 13 illustrates the experimental results of the conventional MPDPC and proposed per-phase MPDPC with switching state preselection strategy, including phase-a input voltage and input current, phase-a switching patterns, and actual real and reactive powers. In Fig. 13(a) and (b), the input currents are sinusoidal and balanced. Unity power factor is achieved since the input current is in phase with the input voltage. In both Fig. 13(a) and (b), the actual real and reactive power correctly track their reference values at $P^* = 500$W and $Q^* = 0$ var, respectively. Both conventional and proposed methods exhibit similar ripples in actual real and reactive power. In terms of switching patterns, it can be seen in Fig. 13(b) that the switching pattern of phase-a contains clamping regions, where the switches in phase-a are prevented from changing the current state. These clamping regions have a value of one-third of the fundamental period, which leads to the total clamping region of phase-a is 240°. This allows the leg having the highest aging level to achieve the minimum switching loss, resulting in an increasing corresponding lifetime. These clamping regions are the difference between the proposed MPDPC scheme with switching state preselection strategy and the conventional method. The frequency spectra of the phase-a input current obtained by the conventional and proposed methods are illustrated in Fig. 13. The THD of the proposed method is slightly higher than that of the conventional scheme. By observing the experimental waveforms, it is apparent that they are closely similar to the simulation results. This serves to confirm the precision of the proposed technique.

The dynamic performance of two control scheme is assessed in Fig. 8, where a step change in the reference real power P^* is made, shifting from 350W to 500W. As shown in Fig. 14, both two control schemes achieve similar power tracking capability. Additionally, the real and reactive powers show no coupling in two control schemes. The switching pattern of phase-a has corrected clamping regions of 120° even during the transient-state, as shown in Fig. 14(b).

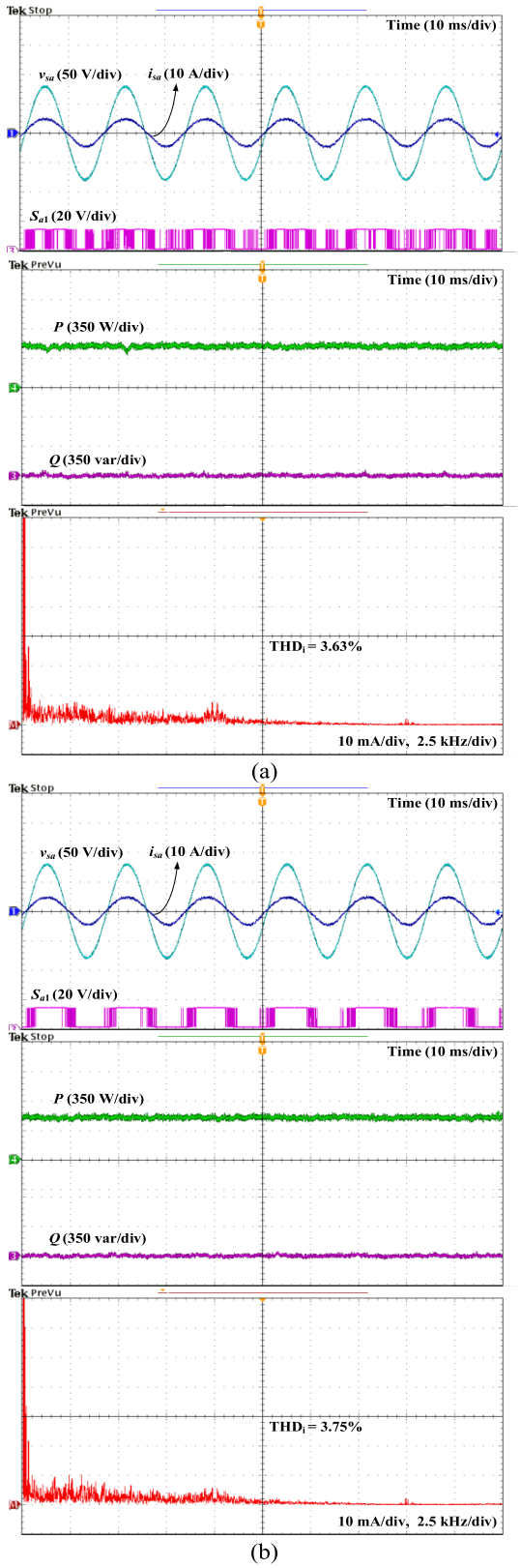

FIGURE 13. Experimental waveform under steady-state condition acquired by (a) the conventional MPDPC, (b) proposed per-phase MPDPC with switching state preselection strategy.

Fig. 15 displays the dynamic response when the reactive power reference Q^* is altered, transitioning from 0 var

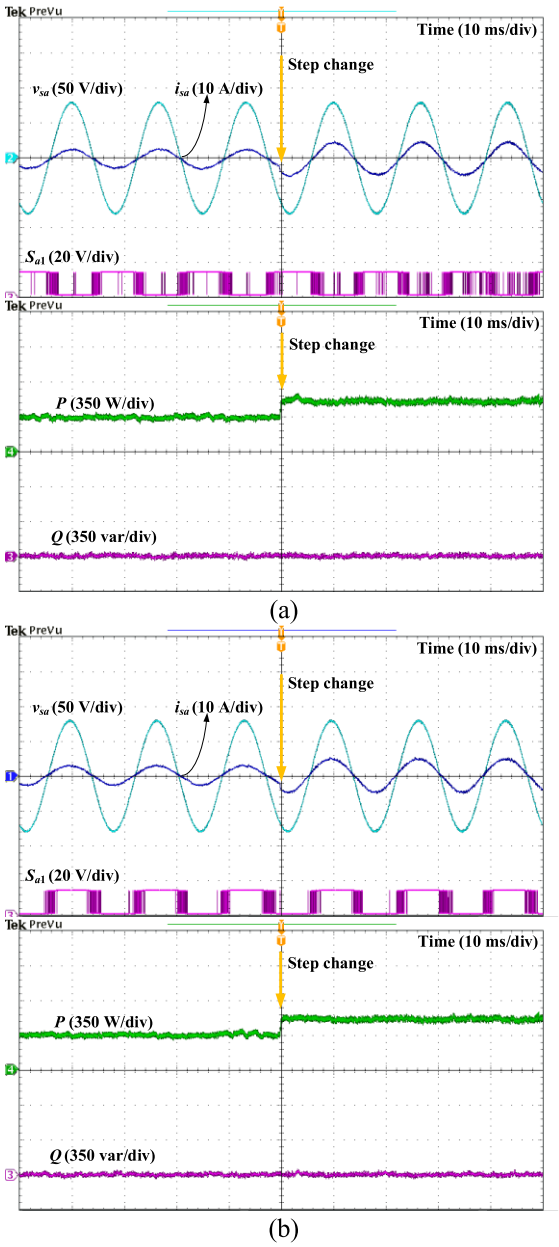

FIGURE 14. Experimental waveform under transient-state condition with increase of real power reference acquired by (a) the conventional MPDPC, (b) proposed per-phase MPDPC with switching state preselection strategy.

to 150 var, while keeping the reference real power fixed at $P^* = 500$W. As shown in Fig. 15, both two control schemes achieve similar power tracking capability. The phase difference between input current and input voltage changes correctly following the rise of reactive power. The switching pattern of phase-a includes correct clamping regions of 120° even during the transient-state.

Fig. 16 shows the behavior of active rectifier under line inductance uncertainty obtained by the proposed method under two conditions. Fig. 16(a) presents the waveforms under the model line inductance as half of real line inductance ($L_{s,model} = 0.5L_{s,real}$), whereas Fig. 16(b) shows the

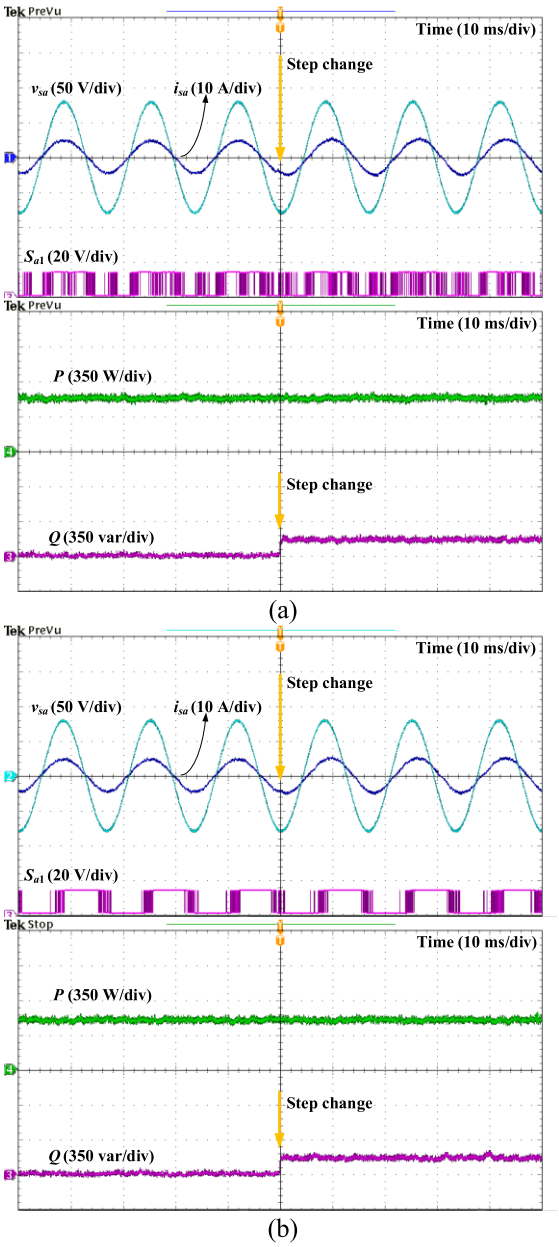

FIGURE 15. Experimental waveform under transient-state condition with increase of reactive power reference acquired by (a) the conventional MPDPC, (b) proposed per-phase MPDPC with switching state preselection strategy.

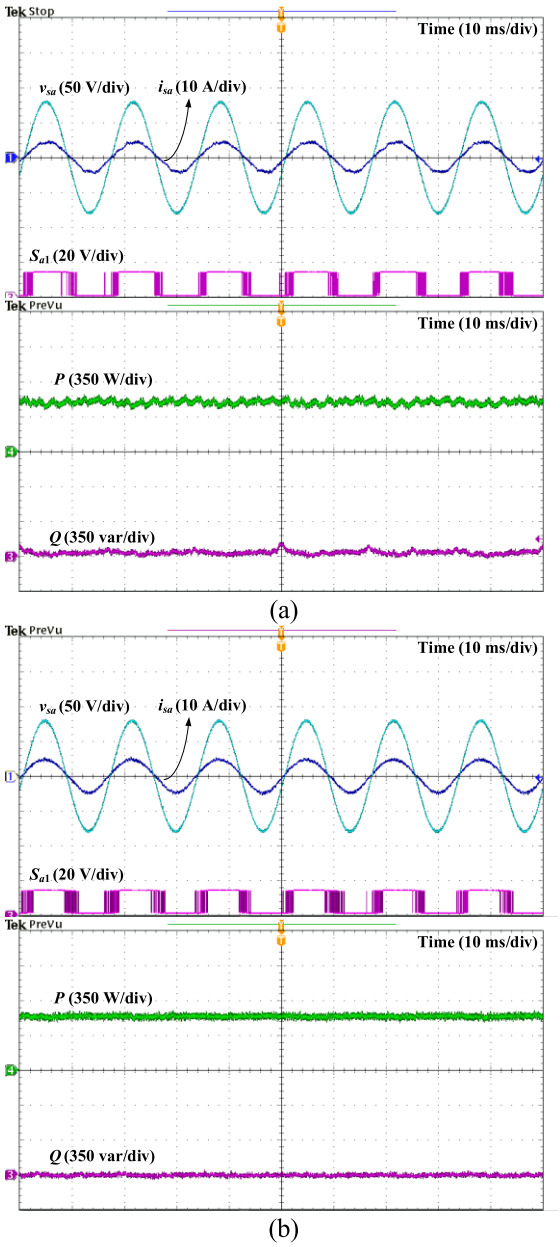

FIGURE 16. Experimental waveform under line inductance uncertainty obtained by proposed per-phase MPDPC with switching state preselection strategy with (a) $L_{s,model} = 50\%L_{s,real}$, (b) (a) $L_{s,model} = 150\%L_{s,real}$.

waveforms under the condition where the model line inductance is 1.5 times higher than the real inductance ($L_{s,model} = 1.5L_{s,real}$). In Fig. 16(a) and (b), the proposed method properly controls the input currents with accurate magnitude and phase. However, it can be noticed that the ripple in real and reactive powers under $L_{s,model} = 0.5L_{s,real}$ condition is higher than that of $L_{s,model} = 1.5L_{s,real}$ condition.

C. PERFORMANCE COMPARISON

The performance between conventional MPDPC method and the proposed MPDPC with switching state preselection strategy are comprehensively evaluated regarding input current THD, switching frequency, power loss, and peak-to-peak ripple of real and reactive powers, as shown in Fig. 17(a) – (f). The power loss of active rectifier includes conduction loss and switching loss, which is calculated following a thermal calculation application note in [36]. Here, the measured input currents and dc-link voltage in the experiment are used along with SKM75GB07E3 IGBT information from the manufacturer's datasheet [37]. As shown in Fig. 17(a), the phase-*a* input current THD attained by the proposed technique is a little higher than the conventional method, whereas the average THD value acquired by the two methods is similar.

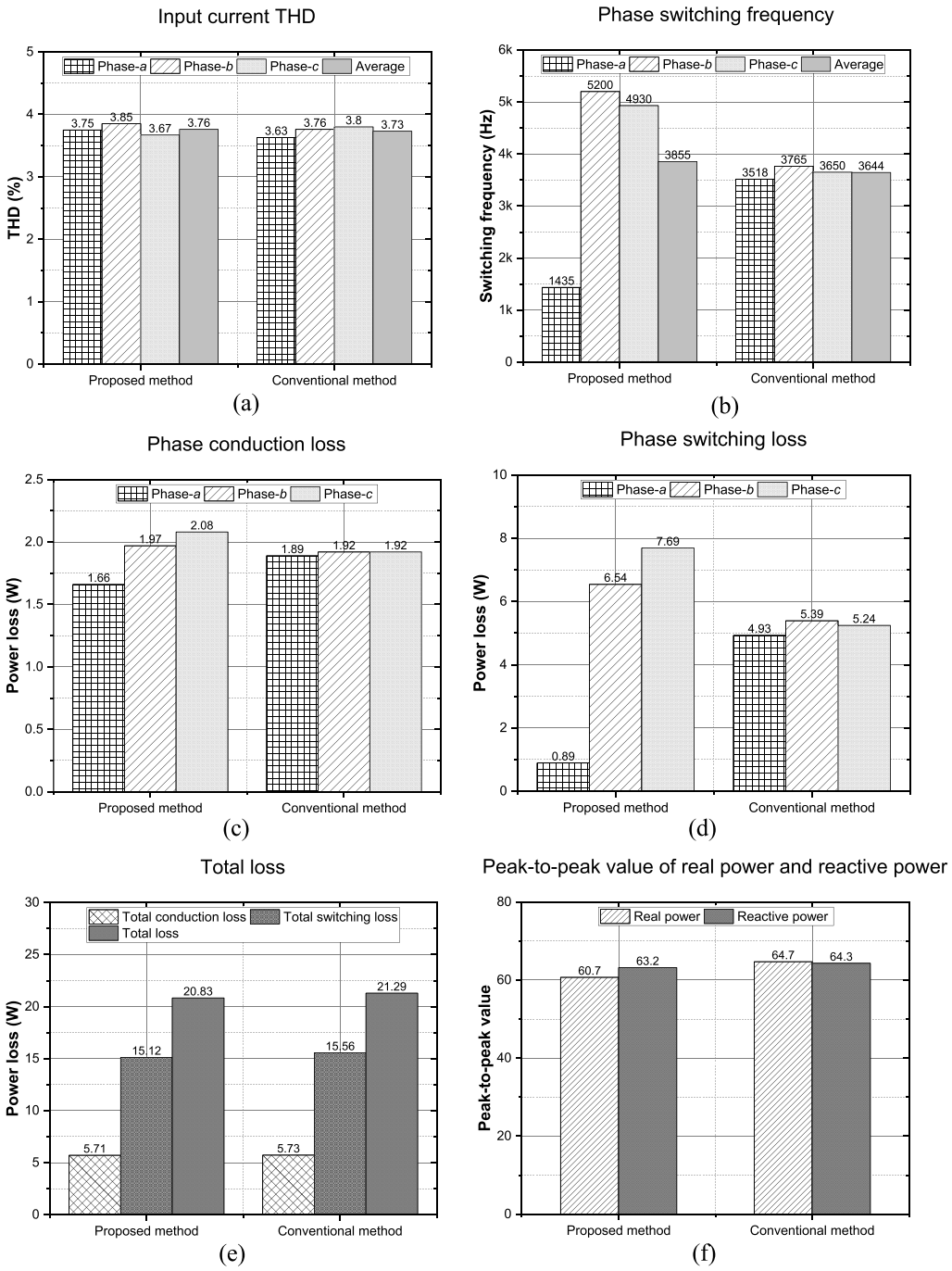

FIGURE 17. **Performance comparison between proposed and conventional methods in terms of (a) input current THD, (b) phase switching frequency, (c) phase conduction loss, (d) phase switching loss, (e) total loss, (f) peak-to-peak value real power and reactive power.**

Because of the clamping regions in phase-*a* obtained by the proposed MPDPC technique, the corresponding switching frequency in phase-*a* is lowered by approximately 60% in comparison to the conventional scheme. However, the switching frequencies in remaining legs obtained by the proposed scheme rise by about 35% in comparison to the conventional method. However, this helps to achieve a similar aging level between phase legs in active rectifier. The average switching frequency acquired by the proposed technique is slightly higher than that of conventional method at about 5%. In terms of conduction loss, there is no significant difference between the two control schemes. Meanwhile, the proposed per-phase MPDPC method significantly lowers the switching loss in phase-*a* by about 81% compared to the conventional method. However, as indicated before, due to the rise of switching frequency in the remaining legs when operating

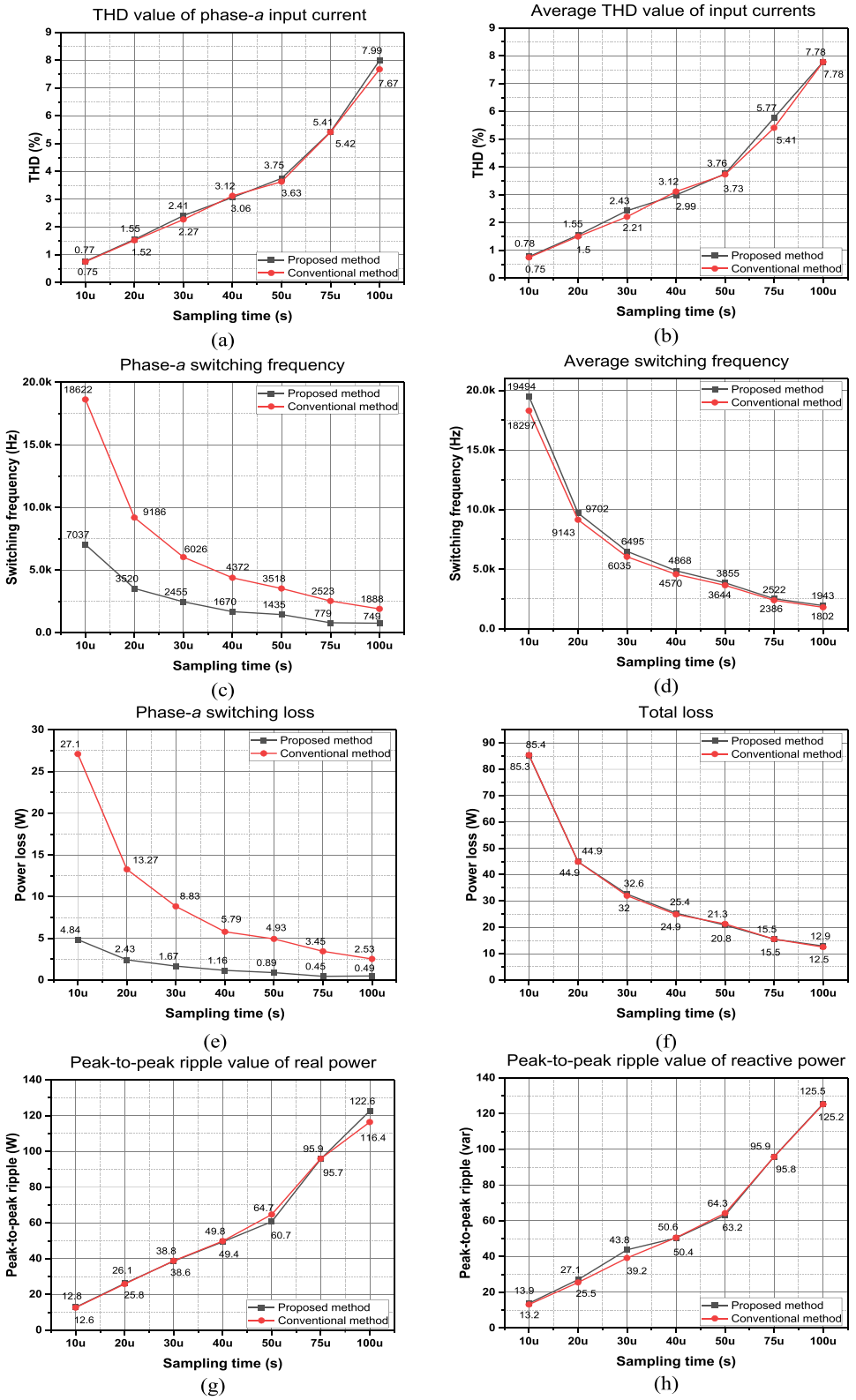

FIGURE 18. Performance comparison between proposed and conventional methods under the change of sampling time (a) phase-a input current THD, (b) average input current THD, (c) phase-a switching frequency, (d) average switching frequency, (e) phase-a switching loss, (f) total loss, (g) peak-to-peak ripple of real power, (h) peak-to-peak ripple of reactive power.

the proposed scheme, the corresponding switching losses in phase-*b* and phase-*c* are higher than that of conventional MPDPC scheme by about 21% and 47%, respectively. Hence, the total loss comparison between the two control schemes

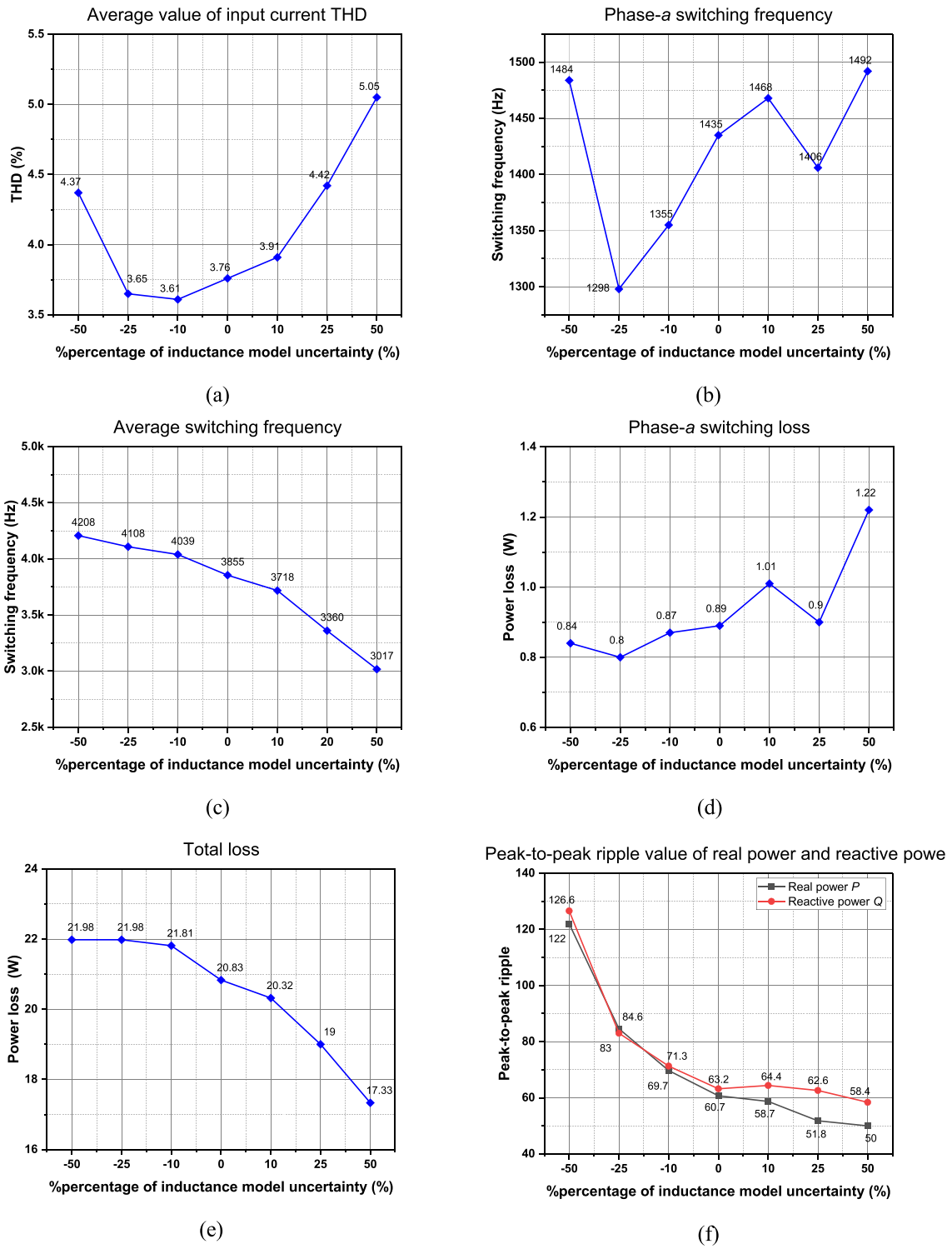

FIGURE 19. Performance of proposed MPDPC method under the line inductance uncertainty (a) average input current THD, (b) phase-a switching frequency, (c) average switching frequency, (d) phase-a switching loss, (e) total loss, (f) peak-to-peak ripple of real power and reactive power.

shown in Fig. 17(e) indicates a similar total loss. In Fig. 17(f), the peak-to-peak ripple of real power and reactive power acquired by the proposed control scheme is vaguely lower than that of the conventional technique.

The comparison between the two methods is further evaluated by implementing them under different sampling times. Fig. 18(a) – (h) shows different performance aspects, including input current THD, switching frequency, power loss, and

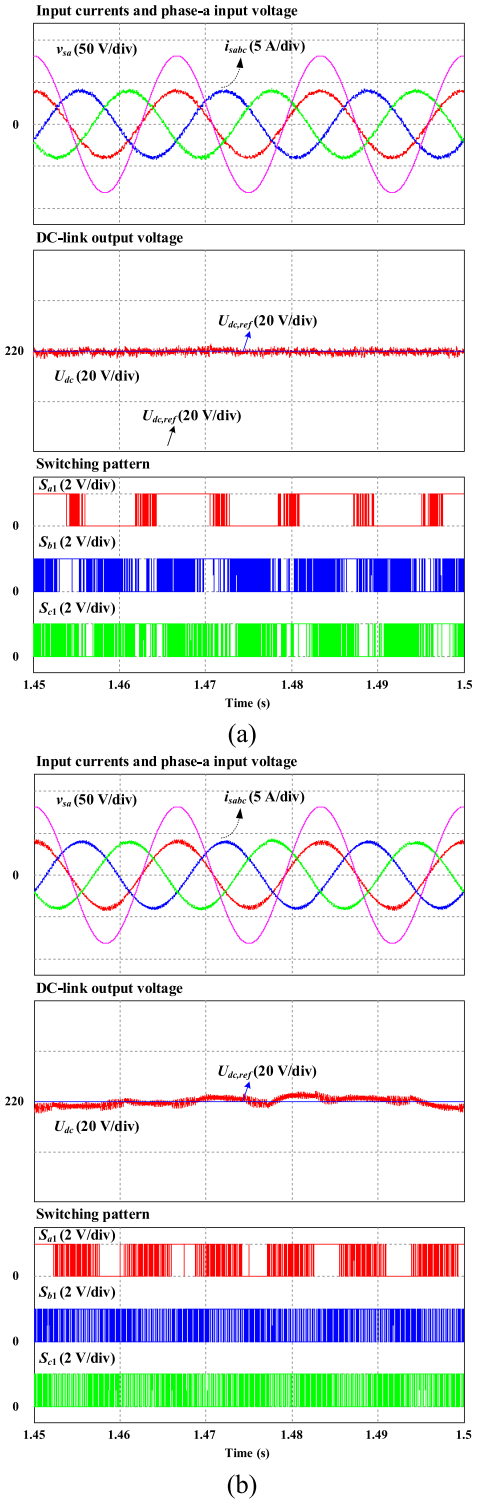

FIGURE 20. Simulation waveforms under transient state condition obtained by (a) proposed per-phase MPDPC with switching state preselection strategy, (b) modified CBPWM.

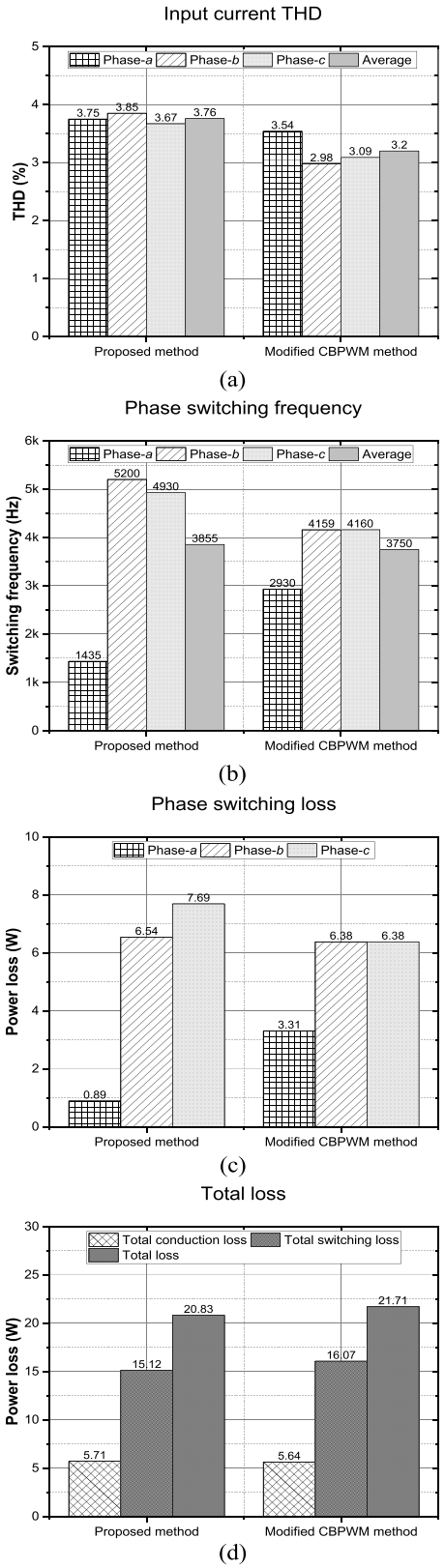

FIGURE 21. Performance comparison between proposed and conventional methods in terms of (a) input current THD, (b) phase switching frequency, (c) phase switching loss, (d) total loss.

peak-to-peak ripple of real power and reactive power acquired by two schemes under the rise of sampling time. It should be noted that the shorter sampling time, the higher output performance. Fig. 18(a) and (b) show the phase-*a* input current THD and average THD values obtained by two control schemes. It can be noticed that the THD increases along with the rise

of sampling time, and the THD values obtained from both approaches are comparable. The switching frequency will decrease when the sampling time increases. Regarding the individual phase switching frequency reduction capability, the proposed technique decreases the switching frequency of phase-a by about 60% in comparison to the conventional method under different sampling times. Meanwhile in Fig. 18(d), the average switching frequency of the proposed method is a little greater compared to conventional method. The per-phase MPDPC scheme decreases the switching loss of phase-a by approximately 81% compared to the conventional method under different sampling time conditions in Fig.18(e). Meanwhile, the total loss obtained by both approaches under different sampling time conditions is similar. The peak-to-peak ripple value of real power and reactive power in Fig. 18(g) and (h) obtained by the two methods have negligible differences.

Fig. 19(a) – (f) presents the performance of proposed technique when there exists parameter uncertainty in line inductance. This performance evaluation includes average THD value, switching frequency and switching loss in phase-a, total loss, and peak-to-peak value ripple in real and reactive power. As shown in Fig. 19(a), the average THD value notably rises under the condition where the model line inductance exceeds the real one, and the model line inductance is lower than the real line inductance by 50%. Meanwhile, the change of phase-a switching frequency under different % percentage of model inductance uncertainty is varied. In these cases, the phase-a switching frequency is lowest when the model line inductance is 25% less than the real one. However, the average switching frequency rises when the model inductance is lower than the real line inductance. This is opposite to the condition that the model inductance exceeds the real one. This behavior is similar to the total loss performance, as shown in Fig. 19(e). In Fig. 19(f), the peak-to-peak ripple values in real and reactive power significantly increase when model line inductance is lower than the real line inductance. The peak-to-peak ripple values in real and reactive power decrease when model line inductance is higher than the real line inductance.

In addition to the comparison between the proposed and conventional methods, a comparison between the proposed per-phase MPDPC with switching state preselection strategy and the individual loss reduction technique based on CBPWM in [20] is implemented. Since the regular MPC method chooses the optimal switching that minimizes a cost function, no commutations are forced every sample period. In fact, one switching state can be the optimal selection for two or more sample periods. This leads to a variable switching frequency. The average switching frequency per power device, f_{sw_avg}, will be defined as the average value of the switching frequencies of the six controlled power semiconductor devices in the active rectifier circuit. Thus,

$$f_{sw\_avg} = \sum_{i=1}^{2} \frac{f_{S_{ai}} + f_{S_{bi}} + f_{S_{ci}}}{6} \tag{19}$$

where $f_{S_{xi}}$ is the switching frequency during a time interval of the power semiconductor device number $i(i = 1, 2)$ of phase $x(x = a, b, c)$. For a fair comparison, the carrier frequency, f_c, and the sampling frequency, f_{sp}, are set to achieve a similar average switching frequency in both the per-phase MPDPC with switching state preselection strategy and the modified CBPWM method in [20].

Fig. 20(a) and 20(b) illustrate the simulation waveforms obtained by the proposed per-phase MPDPC with switching state preselection strategy and modified CBPWM, respectively. As can be seen in Fig. 20, both two methods generate sinusoidal input currents, where the input current is in phase with the input voltage. The dc-link output voltage yielded by the two approaches correctly follows the corresponding reference voltage. It can be seen in Fig. 20(b), the dc-link output voltage acquired by the modified CBPWM has higher fluctuation than that of proposed per-phase MPDPC method. In terms of switching patterns, due to the control scheme in modifying the DPWM1 method, the clamping regions in phase-a have a duration of 60°, whereas the switching pattern of phase-a obtained by the proposed per-phase MPDPC method contains a correct clamping region of 120°.

Fig. 21 shows the performance comparison between proposed per-phase MPDPC with switching state preselection strategy and modified CBPWM. As can be seen in Fig. 21(a), the modified CBPWM method has a lower input current THD than proposed method. As indicated earlier, the carrier frequency, f_c, and the sampling frequency, f_{sp}, are set to achieve a similar average switching frequency in both the per-phase MPDPC with switching state preselection strategy and the modified CBPWM method. Thus, the average switching frequency in both two control schemes is similar, as shown in Fig. 21(b). However, phase-a switching frequency obtained by the proposed method is lower than that of modified CBPWM by about 50% due to the longer clamping time. Due to the reduction of switching frequency, phase-a switching loss obtained by the proposed method is lower than that of modified CBPWM by about 73%, as observed in Fig. 21(c). The total conduction loss obtained by the two approaches is similar, whereas the total loss of modified CBPWM is slightly higher than that of proposed strategy.

V. CONCLUSION

This paper describes the per-phase MPDPC with switching state preselection strategy to control the active rectifier. The method determines the clamping regions and corresponding switching states that maintain the current state of switches in the leg having highest aging level leg, resulting in a decrease of switching loss. The accuracy and feasibility of the proposed per-phase MPDPC technique have been validated both in simulation and in experimentation. It has been demonstrated that the proposed method can substantially reduce switching losses in the phase leg with the highest aging level, achieving a reduction of up to 81% compared to the conventional MPDPC technique. The switching loss of the leg having highest aging level leg is minimal due to the maximum total clamping region, which equals two-thirds of

the fundamental period. Aside from the increased switching losses in the remaining legs, the difference in aging levels among phase legs is decreased, and the total loss in both the conventional and proposed methods is approximately the same. The proposed per-phase MPDPC technique can be integrated into a practical system with ease, offering the potential to deliver benefits across various industries and applications.

REFERENCES

[1] J. R. Rodriguez, J. W. Dixon, J. R. Espinoza, J. Pontt, and P. Lezana, "PWM regenerative rectifiers: State of the art," *IEEE Trans. Ind. Electron.*, vol. 52, no. 1, pp. 5–22, Feb. 2005, doi: 10.1109/TIE.2004.841149.

[2] T. Friedli, M. Hartmann, and J. W. Kolar, "The essence of three-phase PFC rectifier systems—Part II," *IEEE Trans. Power Electron.*, vol. 29, no. 2, pp. 543–560, Feb. 2014, doi: 10.1109/TPEL.2013.2258472.

[3] V. Smet, F. Forest, J.-J. Huselstein, F. Richardeau, Z. Khatir, S. Lefebvre, and M. Berkani, "Ageing and failure modes of IGBT modules in high-temperature power cycling," *IEEE Trans. Ind. Electron.*, vol. 58, no. 10, pp. 4931–4941, Oct. 2011, doi: 10.1109/TIE.2011.2114313.

[4] M. Rodríguez, A. Rodríguez, P. F. Miaja, D. G. Lamar, and J. S. Zuniga, "An insight into the switching process of power MOSFETs: An improved analytical losses model," *IEEE Trans. Power Electron.*, vol. 25, no. 6, pp. 1626–1640, Jun. 2010, doi: 10.1109/TPEL.2010.2040852.

[5] M. Nagao and K. Harada, "Inductor commutation soft-switched PWM inverter driven by frequency-modulated PWM signal," *IEEE Trans. Power Electron.*, vol. 13, no. 1, pp. 67–74, Jan. 1998, doi: 10.1109/63.654960.

[6] L. Chen, A. Amirahmadi, Q. Zhang, N. Kutkut, and I. Batarseh, "Design and implementation of three-phase two-stage grid-connected module integrated converter," *IEEE Trans. Power Electron.*, vol. 29, no. 8, pp. 3881–3892, Aug. 2014, doi: 10.1109/TPEL.2013.2294933.

[7] N. Surasak and H. Fujita, "Current ripple reduction method in a three-phase diode rectifier with an instantaneous reactive power compensator," *IEEE Trans. Ind. Appl.*, vol. 58, no. 3, pp. 3808–3818, May 2022, doi: 10.1109/TIA.2022.3160126.

[8] D.-W. Chung and S.-K. Sul, "Minimum-loss strategy for three-phase PWM rectifier," *IEEE Trans. Ind. Electron.*, vol. 46, no. 3, pp. 517–526, Jun. 1999, doi: 10.1109/41.767058.

[9] L. Asiminoaei, P. Rodriguez, F. Blaabjerg, and M. Malinowski, "Reduction of switching losses in active power filters with a new generalized discontinuous-PWM strategy," *IEEE Trans. Ind. Electron.*, vol. 55, no. 1, pp. 467–471, Jan. 2008, doi: 10.1109/TIE.2007.896554.

[10] R. Jose and C. Patricio, "Control of an active front-end rectifier," in *Predictive Control of Power Converters and Electrical Drives*. Chichester, U.K.: Wiley, 2012, pp. 81–98.

[11] J.-C. Kim and S. Kwak, "Model predictive virtual flux control to improve performance under distorted input voltage conditions," *IEEE Access*, vol. 6, pp. 34921–34933, 2018, doi: 10.1109/ACCESS.2018.2846770.

[12] F. Yu, X. Liu, X. Zhang, and Z. Zhu, "Model predictive virtual-flux control of three-phase Vienna rectifier without voltage sensors," *IEEE Access*, vol. 7, pp. 169338–169349, 2019, doi: 10.1109/ACCESS.2019.2956096.

[13] P. CortÉs, J. RodrÌguez, P. Antoniewicz, and M. Kazmierkowski, "Direct power control of an AFE using predictive control," *IEEE Trans. Power Electron.*, vol. 23, no. 5, pp. 2516–2523, Sep. 2008, doi: 10.1109/TPEL.2008.2002065.

[14] D.-K. Choi and K.-B. Lee, "Dynamic performance improvement of AC/DC converter using model predictive direct power control with finite control set," *IEEE Trans. Ind. Electron.*, vol. 62, no. 2, pp. 757–767, Feb. 2015, doi: 10.1109/TIE.2014.2352214.

[15] P. Antoniewicz and M. P. Kazmierkowski, "Virtual-Flux-Based predictive direct power control of AC/DC converters with online inductance estimation," *IEEE Trans. Ind. Electron.*, vol. 55, no. 12, pp. 4381–4390, Dec. 2008, doi: 10.1109/TIE.2008.2007519.

[16] M. H. Saeedinia and S. A. Davari, "Virtual flux model predictive direct power control (VF-MPDPC) of afe rectifier with new current prediction method and negative sequence elimination," in *Proc. IEEE Int. Symp. Predictive Control Electr. Drives Power Electron. (PRECEDE)*, Sep. 2017, pp. 113–118, doi: 10.1109/PRECEDE.2017.8071278.

[17] J. Sawma, F. Khatounian, E. Monmasson, L. Idkhajine, and R. Ghosn, "Cascaded Dual-Model-Predictive control of an active front-end rectifier," *IEEE Trans. Ind. Electron.*, vol. 63, no. 7, pp. 4604–4614, Jul. 2016, doi: 10.1109/TIE.2016.2547874.

[18] M. Gendrin, J.-Y. Gauthier, and X. Lin-Shi, "A predictive hybrid Pulse-Width-Modulation technique for Active-Front-End rectifiers," *IEEE Trans. Power Electron.*, vol. 32, no. 7, pp. 5487–5496, Jul. 2017, doi: 10.1109/TPEL.2016.2612832.

[19] S. Kwak and J.-C. Park, "Model-predictive direct power control with vector preselection technique for highly efficient active rectifiers," *IEEE Trans. Ind. Informat.*, vol. 11, no. 1, pp. 44–52, Feb. 2015, doi: 10.1109/TII.2014.2363761.

[20] M.-H. Nguyen, S. Kwak, and S. Choi, "Individual loss reduction technique for each phase in three-phase voltage source rectifier based on carrier-based pulse-width modulation," *J. Electr. Eng. Technol.*, Aug. 2023, doi: 10.1007/s42835-023-01604-x.

[21] M.-H. Nguyen, S. Kwak, and S. Choi, "Model predictive control algorithm for prolonging lifetime of three-phase voltage source converters," *IEEE Access*, vol. 11, pp. 72781–72802, 2023, doi: 10.1109/ACCESS.2023.3294995.

[22] M. H. Nguyen, S. Kwak, and S. Choi, "Lifetime extension technique for voltage source inverters using selected switching states-based MPC method," *IEEE Access*, vol. 11, pp. 88686–88702, 2023, doi: 10.1109/ACCESS.2023.3302924.

[23] R. Jose and C. Patricio, "Cost function selection," in *Predictive Control of Power Converters and Electrical Drives*. Chichester, U.K.: Wiley, 2012, pp. 145–161.

[24] K. Liao, D. Lu, M. Wang, and J. Yang, "A low-pass virtual filter for output power smoothing of wind energy conversion systems," *IEEE Trans. Ind. Electron.*, vol. 69, no. 12, pp. 12874–12885, Dec. 2022, doi: 10.1109/TIE.2021.3139177.

[25] X. Lin, Y. Wen, R. Yu, J. Yu, and H. Wen, "Improved weak grids synchronization unit for passivity enhancement of grid-connected inverter," *IEEE J. Emerg. Sel. Topics Power Electron.*, vol. 10, no. 6, pp. 7084–7097, Dec. 2022, doi: 10.1109/JESTPE.2022.3168655.

[26] X. Lin, Y. Liu, J. Yu, R. Yu, J. Zhang, and H. Wen, "Stability analysis of three-phase grid-connected inverter under the weak grids with asymmetrical grid impedance by LTP theory in time domain," *Int. J. Electr. Power Energy Syst.*, vol. 142, Nov. 2022, Art. no. 108244, doi: 10.1016/j.ijepes.2022.108244.

[27] Y. Shen, D. Liu, W. Liang, and X. Zhang, "Current reconstruction of three-phase voltage source inverters considering current ripple," *IEEE Trans. Transport. Electrific.*, vol. 9, no. 1, pp. 1416–1427, Mar. 2023, doi: 10.1109/TTE.2022.3199431.

[28] V. Smet, F. Forest, J.-J. Huselstein, A. Rashed, and F. Richardeau, "Evaluation of V_{ce} monitoring as a real-time method to estimate aging of bond wire-IGBT modules stressed by power cycling," *IEEE Trans. Ind. Electron.*, vol. 60, no. 7, pp. 2760–2770, Jul. 2013, doi: 10.1109/TIE.2012.2196894.

[29] Y. Peng and H. Wang, "A simplified on-state voltage measurement circuit for power semiconductor devices," *IEEE Trans. Power Electron.*, vol. 36, no. 10, pp. 10993–10997, Oct. 2021, doi: 10.1109/TPEL.2021.3070698.

[30] A. Eleffendi and C. M. Johnson, "Evaluation of on-state voltage VCE(ON) and threshold voltage vth for real-time health monitoring of IGBT power modules," in *Proc. 17th Eur. Conf. Power Electron. Appl.*, Sep. 2015, pp. 1–10, doi: 10.1109/EPE.2015.7309265.

[31] S. H. Ali, X. Li, A. S. Kamath, and B. Akin, "A simple plug-in circuit for IGBT gate drivers to monitor device aging: Toward smart gate drivers," *IEEE Power Electron. Mag.*, vol. 5, no. 3, pp. 45–55, Sep. 2018, doi: 10.1109/MPEL.2018.2849653.

[32] B. Tian, W. Qiao, Z. Wang, T. Gachovska, and J. L. Hudgins, "Monitoring IGBT's health condition via junction temperature variations," in *Proc. IEEE Appl. Power Electron. Conf. Expo.*, Mar. 2014, pp. 2550–2555, doi: 10.1109/APEC.2014.6803662.

[33] Z. Wang, B. Tian, W. Qiao, and L. Qu, "Real-time aging monitoring for IGBT modules using case temperature," *IEEE Trans. Ind. Electron.*, vol. 63, no. 2, pp. 1168–1178, Feb. 2016, doi: 10.1109/TIE.2015.2497665.

[34] H. Wang, Z. Xu, X. Ge, Y. Liao, Y. Yang, Y. Zhang, B. Yao, and Y. Chai, "A junction temperature monitoring method for IGBT modules based on turn-off voltage with convolutional neural networks," *IEEE Trans. Power Electron.*, vol. 38, no. 8, pp. 10313–10328, Aug. 2023, doi: 10.1109/TPEL.2023.3278675.

[35] *TI Designs: TIDM-1000*. Accessed: Oct. 10, 2023. [Online]. Available: https://www.ti.com/lit/ug/tiducj0b/tiducj0b.pdf

[36] ON Semiconductor, *Appl. Note AND9140/D*, Thermal Calculations for IGBTs, Scottsdale, AZ, USA, Apr. 2014.

[37] *SEMIKRON SKM75GB07E3 Datasheet*, Semikron Danfoss, Essex, U.K., Dec. 2021.

MINH HOANG NGUYEN received the B.S. degree in electrical and electronics engineering from the Hanoi University of Science and Technology, Vietnam, in 2016, and the Ph.D. degree from Chung-Ang University, Seoul, South Korea, in 2023. He is currently a Researcher with Chung-Ang University. His research interests include control for two-level and multilevel converters, and reliability for converter.

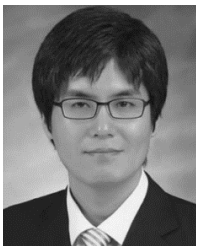

SANGSHIN KWAK (Member, IEEE) received the Ph.D. degree in electrical engineering from Texas A&M University, College Station, TX, USA, in 2005. From 2007 to 2010, he was an Assistant Professor with Daegu University, Gyeongsan, South Korea. Since 2010, he has been with Chung-Ang University, Seoul, South Korea, where he is currently a Professor. His current research interests include the design, modeling, control, and analysis of power converters for electric vehicles and renewable energy systems as well as the prognosis and fault tolerant control of power electronics systems.

SEUNGDEOG CHOI (Senior Member, IEEE) received the B.S. degree in electrical and computer engineering from Chung-Ang University, Seoul, South Korea, in 2004, the M.S. degree in electrical and computer engineering from Seoul National University, Seoul, in 2006, and the Ph.D. degree in electric power and power electronics from Texas A&M University, College Station, TX, USA, in 2010. From 2006 to 2007, he was a Research Engineer with LG Electronics, Seoul. From 2009 to 2012, he was a Research Engineer with Toshiba International Corporation, Houston, TX, USA. From 2012 to 2018, he was an Assistant Professor with The University of Akron, Akron, OH, USA. Since 2018, he has been an Associate Professor with Mississippi State University, Starkville, MS, USA. His current research interests include degradation modeling, fault tolerant control, and fault tolerant design of electric machines, power electronics, batteries, solar panels, and wider vehicular/aircraft microgrid systems.